Title

Recurrent dynamics of rupture transitions of giant lipid vesicles at solid surfaces

Journal

Biophysical Journal, 120(4)

ISSN

0006-3495

Authors

Ngassam, Viviane N
Su, Wan-Chih
Gettel, Douglas L
et al.

Publication Date

2021-02-01

DOI

10.1016/j.bpj.2021.01.006

Peer reviewed

Biophysical Journal
Article

Biophysical Society

Recurrent dynamics of rupture transitions of giant lipid vesicles at solid surfaces

Viviane N. Ngassam,[1] Wan-Chih Su,[2] Douglas L. Gettel,[3] Yawen Deng,[1] Zexu Yang,[1] Neven Wang-Tomic,[1] Varun P. Sharma,[1] Sowmya Purushothaman,[1] and Atul N. Parikh[1,2,3,4,*]

[1]Department of Biomedical Engineering, University of California, Davis, California; [2]Department of Chemistry, University of California, Davis, California; [3]Department of Chemical Engineering, University of California, Davis, California; and [4]Department of Materials Science and Engineering, University of California, Davis, California

ABSTRACT Single giant unilamellar vesicles (GUVs) rupture spontaneously from their salt-laden suspension onto solid surfaces. At hydrophobic surfaces, the GUVs rupture via a recurrent, bouncing ball rhythm. During each contact, the GUVs, rendered tense by the substrate interactions, porate, and spread a molecularly transformed motif of a monomolecular layer on the hydrophobic surface from the point of contact in a symmetric manner. The competition from pore closure, however, limits the spreading and produces a daughter vesicle, which re-engages with the substrate. At solid hydrophilic surfaces, by contrast, GUVs rupture via a distinctly different recurrent burst-heal dynamics; during burst, single pores nucleate at the contact boundary of the adhering vesicles, facilitating asymmetric spreading and producing a "heart"-shaped membrane patch. During the healing phase, the competing pore closure produces a daughter vesicle. In both cases, the pattern of burst-reseal events repeats multiple times, splashing and spreading the vesicular fragments as bilayer patches at the solid surface in a pulsatory manner. These remarkable recurrent dynamics arise, not because of the elastic properties of the solid surface, but because the competition between membrane spreading and pore healing, prompted by the surface-energy-dependent adhesion, determine the course of the topological transition.

SIGNIFICANCE Giant lipid vesicles adhering to a solid surface experience strong mechanical stresses. The contacting membrane segment loses thermal fluctuations and accumulates mechanical tension, the equilibration of which can give rise to global shape changes, lipid phase separation, and traction forces. Beyond a threshold tension, vesicles porate, unravel, and spread. Here, we find that a competition from pore healing can make rupture iterative rather than a single all-or-nothing event. During burst, single pores expand, spreading a lipid bilayer on the hydrophilic surface and a monolayer on the hydrophobic one. During heal, pore healing can produce daughter vesicles. This burst-reseal event reiterates "splashing" portions of single vesicles at the solid surface and "bouncing" the remainder as a secondary vesicle in multiple steps.

INTRODUCTION

Topologically closed giant vesicles (GUVs) (1–5), isolating femto- to picoliter quantities of aqueous core from the surrounding bulk, are the simplest cell-sized compartments (2) (5–50 μm in diameter). They are delimited by a barrier membrane (6) (4–6 nm thick), which is a self-assembled single lamellae of phospholipid bilayers (7) held together by noncovalent hydrophobic interactions (8). Acting as a highly deformable elastic sheet, the membrane presents a unique combination of elastic properties: low shear modulus ($\sim 10^{-3}$ N $\cdot$ m^{-1}) due to the in-plane lateral fluidity (9); large volume compressibility ($\sim 10^{9}$–10^{10} N $\cdot$ m^{-2}) and large area expansion (10^{2}–10^{3} mN $\cdot$ m^{-1}) moduli, reflecting the cooperative strength of the hydrophobic effect (10); and relatively low bending rigidities (10^{-19} N $\cdot$ m) (11), a few times larger than the thermal energy, $\sim 20\ k_{B}T$ (where $k_{B}T \approx 4 \times 10^{-21}$ J). As a consequence, the membranes of GUVs resist large-scale thickness fluctuations and bend readily but tolerate only a limited area expansion ($\sim$5%) before the cumulated tension fails the membrane and ruptures the vesicle.

In the vicinity of an attractive solid surface, vesicles experience strong mechanical stresses. It is now well established

Submitted June 8, 2020, and accepted for publication January 7, 2021.

*Correspondence: anparikh@ucdavis.edu

Viviane N. Ngassam and Wan-Chih Su contributed equally to this work.

Editor: Rumiana Dimova.

https://doi.org/10.1016/j.bpj.2021.01.006

that the adhesion of GUVs at the solid-liquid interface (12,13) 1) suppresses membrane undulations, rendering membranes mechanically tense (14); 2) elevates intravesicular hydrostatic pressure and generates traction forces (15); 3) increases membrane permeability (16) and drives shape transformations (12); and 4) induces lateral phase separation of membrane components, thus stabilizing membrane heterogeneity (17,18). In a limiting case, when the adhesion energy overcomes the elastic energy penalty against the deformations that occur at the solid-membrane contact line, GUVs rupture at solid surfaces (12,19). Here, the balance between the adhesion energy per unit area, W, and the surface tension, σ—given by Young-Dupre's equilibrium relation $W = \sigma(1 - \cos\theta)$, where θ represents the contact angle at the adhesion rim—stretches the membrane beyond the rupture tension (2–5 mN/m) (20), promoting the formation of a membrane pore through a thermally activated, stochastic nucleation process (21,22). Once a pore opens, the membrane tension can continue to relax via pore expansion, allowing the solid-membrane contact line to spread further, thus facilitating an irreversible topological transition rupturing the GUV at the solid surface and forming a well-defined, quasi-two-dimensional, single lipid bilayer patch terminated by free edges (22,23).

The biophysical mechanisms by which single GUVs rupture at solid surfaces have been a subject of many recent studies (24–28). Using time-lapse fluorescence microscopy, Hamai and co-workers (24–26) monitored the time-dependent progression of physical destabilization of GUVs at solid hydrophilic surfaces and identified multiple different pathways. They found that an overwhelming proportion of vesicles (~92% cases, n = 39) followed a single mode, which they dubbed asymmetric isolated rupture pathway. Here, the rupture proceeds through the nucleation of a pore near the rim of the adsorbed vesicle at the substrate surface. A subsequent expansion of the pore and an abrupt rupture-induced spreading of the membrane (10–20 ms) then resulted in a characteristic heart-shaped bilayer patch.

At hydrophobic surfaces, by contrast, GUVs wet the aqueous interface by a distinctly different mechanism involving a gross structural transformation of the bilayer motif into a monolayer one. A hydrophobic surface in water is characterized by a large surface energy (~40–50 mN/m). This high interfacial energy then provides the driving force for the adhesion of the GUV at a hydrophobic surface. Because the gain in the adhesion energy per unit area (W), comparable to the surface energy, far exceeds the rupture tension (2–5 mN/m) of the vesicular membrane, a GUV wetting a hydrophobic surface ruptures and spreads. The spreading of the lipids from the source GUV releases the hydrophobic surface energy by producing a monomolecular lipid layer, which transforms the hydrophobic interface into a hydrophilic one (26,29,30). The kinetic pathways characterizing the rupture of GUVs at hydrophobic surfaces are reported recently by Zan and co-workers (31) using time-resolved video microscopy. Their results support a mechanism in which a rare event leading to the disruption of the outer leaflet of the adhering GUV initiates the transfer of lipids to the hydrophobic surface, thus creating a precursor "hemifusion diaphragm" at the contact line. This initial loss of lipids from the outer leaflet alone produce a mismatch in molecular densities of the two leaflets, which then tenses the outer leaflet and lowers the energy barrier for pore formation near the contact line. The pore edges facilitate lipid exchange between the leaflets and their eventual transfer to the surface, ultimately transforming the GUV into a monomolecular lipid layer at the hydrophobic surface.

Although different, the two mechanisms characterizing the behaviors of GUVs at hydrophilic and hydrophobic surfaces are both mediated by the formation of a membrane pore, which forms because of the mechanical tension produced by the adhesive interactions between single GUVs and the solid surface. Considering this central role of pore formation in driving vesicle rupture raises a general question: how does the competition from pore healing mediate the rupture process? It is clear that the formation and growth of a pore helps mechanically stressed vesicles relieve membrane tension both by reducing effective membrane area and decreasing the vesicular volume, promoting spreading (32,33). But the pore formation also creates a solvent-exposed free edge. The reorientation of the edge lipids into a hemimicellar configuration driven by hydrophobic forces (34) then accrues mechanical tension at the edge (γ). As a consequence, the internal Laplace pressure ($= 2\sigma/R$), where R corresponds to the radius of the deformed GUV, facilitates the volume loss from the vesicular compartment and promotes membrane healing by pore- closure (32,35). Thus, a balance of the competition between these two effects, spreading and healing (36), must dictate the dynamics and final morphologies produced by the rupture of vesicles at solid surfaces.

Here, we identify a new, to our knowledge, and heretofore unappreciated, feature of surface-mediated rupture of giant vesicles. We find that an interplay between spreading and healing can give rise to nontrivial dynamics characterizing vesicle rupture at the solid-liquid interface. Specifically, we find that when spreading effects due to adhesive interactions do not dominate, the pore-nucleated GUV rupture process is no longer an all-or-nothing event, but rather, it follows a well-orchestrated, iterative sequence of steps in a surface-energy-dependent manner. On low-energy hydrophobic substrates, we find that the symmetric spreading accompanies vesicle rupture. But the GUV rupture is not a singular event. It proceeds in multiple steps via a trampoline-like bouncing ball rhythm in which single vesicles striking the substrate form microscopic pores and spread partially at the point of contact between essentially undeformed GUVs and the underlying hydrophobic substrate before detaching from the surface and bouncing off. The process repeats multiple times before the vesicle membrane is transformed into a lamellar

monolayer adhering firmly to the hydrophobic surface. By contrast, on hydrophilic surfaces, we confirm that GUVs rupture asymmetrically, producing heart-shaped bilayers. Here too, however, the rupture process is intermittent; the transformation of the three-dimensional vesicle into a membrane patch does not conclude with a single rupture. Instead, the rupture process involves a series of repeated burst-heal events characterizing the topological transformation. During the burst regime, single pores nucleating at the contact boundary of the adhering deflated vesicles not only produce the "heart"-shaped patches of lamellar membrane fragments but also give rise to free daughter vesicles, likely by the healing of nonadhering portions of the parent GUV. This burst-reseal event reiterates multiple times, "spilling" portions of single GUV membranes at the solid surface and producing multiple heart-shaped patches of supported membrane patches. In both cases, this cyclical pattern of poration, spreading, and resealing, arising from a competition between adhesion-mediated membrane spreading and pore healing, causes unusual dynamics characterized by wetting, splashing, and bouncing of giant vesicles at solid surfaces in a surface-free-energy-dependent manner.

MATERIALS AND METHODS

Materials

POPC (1-palmitoyl-2-oleoyl-*sn*-glycero-3-phosphocholine) and rhodamine-B DOPE (1,2-dioleoyl-*sn*-glycero-3-phosphoethanolamine-N-(lissamine rhodamine-B sulfonyl)) were purchased from Avanti Polar Lipids (Birmingham, AL). Sucrose, sodium chloride, and potassium chloride were from Fisher Chemical (Fair Lawn, NJ). Glucose, toluene, chloroform, acetone, sulfuric acid, and octadecyltrichlorosilane (OTS), 90+% were purchased from Sigma-Aldrich (Saint Louis, MO); hydrogen peroxide was from EMD Chemicals (Gibbstown, NJ); and Dulbecco phosphate-buffered saline 1× without calcium chloride and without magnesium chloride was purchased from Gibco (Grand Island, NY). All chemicals were used without further purification, and all aqueous solutions were prepared with 18.2 mΩ-cm Milli-Q deionized water.

Preparation of giant vesicles

Giant vesicles were prepared by adapting the well-established electroformation method developed by Angelova and co-workers (37). Small droplets (15–20 μL) of lipid solution in chloroform (2 mg/mL) were spread on an ITO-coated coverslip and allowed to dry under vacuum for at least 2 h. The dried lipid cake was then hydrated with a 300 mM sucrose solution in deionized water and sandwiched using a second ITO slide. GUVs were electroformed by subjecting the sandwich to a 4 V AC sine-wave voltage at 10 Hz for 90 min, followed by a 4 V square wave voltage at 2 Hz for an additional 90 min.

Preparation of hydrophobic substrates

Glass substrates (22 × 22 mm coverslips; Corning, Corning, NY) were cleaned for 3–5 min with piranha etch, a 4:1 mixture of sulfuric acid and hydrogen peroxide heated to 90°C, to remove organic residues. (Caution: this mixture reacts violently with organic materials and must be handled with extreme care.) The substrates were then rinsed copiously with deionized (18 mΩ-cm) water and dried under a stream of nitrogen. The deposition of *n*-OTS ($H_3C(CH_2)_{17}17SiCl_3$) was achieved by adapting a previously described method (30). Briefly, all freshly oxidized coverglass substrates were immersed in a 50 mL of 2.5 mM OTS solution in anhydrous toluene. The substrates were allowed to incubate in the solution for ~45–55 min. All silanization reactions were carried out in glass containers under nominally dry ambient conditions (relative humidity <20%). After removal from the solution, the film-covered substrates were rinsed with chloroform and washed extensively with acetone under ultrasonic conditions to remove any excess reactants. Silanized samples were used within 1–3 days of preparation.

Imaging of GUVs incubated in different osmotic balanced concentrations of salty solutions

Aliquots (15 μL) of freely suspended membranes of sugar-encapsulating GUVs were studied at ambient temperature in either eight-well chambers fitted with a glass bottom coverslip (Nunc, Rochester) or closed chambers fitted with OTS-coated glass coverslips. We chose chambers over the conventional coverslip sandwiches because 1) they reduce the risk of GUV deformation by mechanical pressure; 2) they afford large sample volumes, which reduces the possibility of inadvertent generation of significant osmotic imbalances due to solvent evaporation during extended experimental timescales (e.g., overnight); 3) they enable osmotic gradient generation in real time; and 4) they allow solvent exchange and bilayer formation directly inside the chamber. GUVs were incubated for 10–30 min in 300 mM glucose solution for control, then in 1) 150 mM NaCl, 2) 150 mM KCl, or 3) mixtures of 150 mM glucose and 75 mM NaCl.

Fluorescence microscopy measurements

Vesicles were monitored in real time using either epifluorescence microscopy (Nikon Eclipse TE2000 inverted fluorescence microscope (Technical Instruments, Burlingame, CA) equipped with a Roper Cool Snap camera (Technical Instruments) and an Hg lamp as the light source) or a fluorescence microscope equipped with spinning disk confocal configuration using an Intelligent Imaging Innovations Marianas Digital Microscopy Workstation (3i; Denver, CO) fitted with a CSU-X1 spinning disk head (Yokogawa Musashino, Tokyo, Japan) and a QuantEM512SC electron-multiplying charge-coupled device (EMCCD) camera (Photometrics, Tuscon, AZ). Fluorescence micrographs were obtained using oil immersion objectives (Zeiss Fluor 40× (NA 1.3), Zeiss Plan-Fluor 63× (NA 1.4), and Zeiss Fluor 100× (NA 1.46); Carl Zeiss Oberkochen, Germany). Rhodamine-B DOPE (Ex/Em; 560/583) was exposed with a 5 mW 561 laser line. ImageJ (https://rsbweb.nih.gov/ij/), a public-domain software, and Slidebook digital microscopy imaging software (3i) were used.

FRAP measurements

Fluorescence recovery after photobleaching (FRAP) experiments were performed with a 5 mW 561 laser line. Vesicles were viewed in the equatorial plane with a 40× objective and a QuantEM512SC EMCCD camera, giving a 512 × 512 pixel image. Rhodamine-B DOPE fluorescent probes were bleached in a circular region (~3.2 μm in radius) at 100% of maximal laser power. Recovery of fluorescence was recorded and measured from the subsequent 250 frames, 10 frames per second. The diffusion coefficient was calculated as $\boldsymbol{D} = (\boldsymbol{r}^2/4 \times \boldsymbol{t}_{1/2})$, where r is the radius of the bleached spot and $\boldsymbol{t}_{1/2}$ is the half-time of recovery (38).

RESULTS AND DISCUSSION

General remarks

For our study, we used electroformed giant vesicles (GUVs, 20–50 μm in diameter) (4,5) consisting primarily of a

common unsaturated phospholipid, namely POPC, and encapsulating 100–300 mM sucrose under room temperature (~23.0 (± 0.5)°C) conditions (Materials and methods). For real-time visualization of the membrane by time-resolved fluorescence microscopy, we doped the GUVs with a small concentration (≤1.0 mol%) of a probe lipid, namely rhodamine-B DOPE (39). Transferring the sucrose-laden GUVs to an osmotically balanced bath containing isomolar concentrations of less dense glucose facilitates their gravitational settlement onto the underlying surface. Under these conditions, the GUVs gravitating toward the underlying surface, hydrophilic and hydrophobic alike, remain largely undeformed, retaining their spherical shape and exhibiting bending-dominated and thermally excited topographical undulations (Video S1). By contrast, when the extravesicular dispersion medium, although osmotically balanced, contained even a small concentration of sodium chloride (≥5 mM), the GUVs adhere to the underlying surface, likely by overcoming the hydration, undulation, and electrostatic repulsion (19). In what follows, we describe the behaviors of GUVs at surfaces as revealed by time-lapse fluorescence microscopy. We begin with the results describing the behavior of GUVs in salt-laden solutions at hydrophobic surface, which involves a gross motif transformation followed by that on more commonly employed hydrophilic surface.

Rupture of single GUVs at extended hydrophobic surfaces

A representative time-lapse video and a corresponding montage of selected frames of epifluorescence micrographs (Figs. 1 and S1; Video S2) of GUVs settling onto OTS derivatized, hydrophobic glass surface (see Materials and methods) document this progression. Upon contacting the surface, the GUVs undergo an abrupt topological transition, abandoning their topologically closed motif and producing a rapidly spreading lipid layer adhering to the substrate surface in a radially symmetric manner, in full agreement with previous reports of lipid spreading producing a monomolecular lipid layer at the hydrophobic surface (31). The spreading persists for 400–500 s, ultimately producing a circular lipid patch adhering to the underlying hydrophobic surface. Quantifying the rate at which the lipid layer spreads at the substrate surface, we find the areal spreading rate of $(dA/dt) = 193 \pm 77$ standard deviation (SD) $\mu m^2/s$, n = 3 (Fig. 1 *b*), which is of the same order of magnitude reported previously for the spreading of the more fluid DOPC membrane (738 ± 29 SD $\mu m^2/s$) (31).

A closer view of the GUV and the surface provide previously unappreciated details of the vesicle rupture process. Examining the fate of the GUVs during its interaction with the hydrophobic surface, we see that the parent GUV largely retains its overall spherical shape (at the optical length scale) and exhibits a gradual decrease in size. An analysis of the time-lapse images reveals the decay of vesicle size is not strictly monotonic (Fig. 1 *c*), but rather that the vesicle size decreases in a stepwise manner, creating a staircase-shaped profile. During each step, vesicle diameters decreases gradually for ~20–30 s before reaching the next plateau, which lasts for ~10–15 s. Moreover, at each plateau or each rung of the staircase profile, a single microscopic (2–4 μm in diameter) transient pore (Fig. 1 *c*; Video S3), lasting hundreds of milliseconds, is visible. Comparing multiple steps of the single vesicles further reveal that the pores appear randomly over the nonadhering part of the vesicle. Together, these observations indicate that vesicle rupture at hydrophobic surface is not a singular event. Instead, a cascade of ruptures, each releasing a fraction of the membrane material from the parent GUV to the solid surface, characterizes vesicle rupture. In other words, the spreading of GUVs onto a hydrophobic surface follows a heretofore unappreciated recurrent nature of the rupture dynamics; the membrane spreads, stalls, and spreads again.

The spreading of lipids at the high-energy aqueous interface of hydrophobic solids proceeds under a tension gradient ($\Delta\sigma$) reminiscent of Marangoni flow (40). Previous studies have established that the balance between this Marangoni stress and the frictional dissipation at the spreading front then characterizes the dynamics of lipid spreading ($\Delta\sigma = \zeta v$, where ζ is the frictional coefficient and v the spreading velocity) (41,42). This yields an inverse square-root dependence of spreading velocity on time: $v = \sqrt{\beta/t}$, with a kinetic spreading coefficient $\beta = (S/2\zeta)$, where S represents the spreading power given by the difference in free energy between lipids on the surface and those in the precursor GUV. Adapting previously reported analyses of spreading kinetics, the time-dependent 1) radius of the circularly spreading monolayer on hydrophobic surface is $R(dR/dt)ln(R/\varepsilon) = 2\beta$ (40) and 2) area is $A(t) = \pi R(t)^2 = (4\pi\beta/ln(R(t)/\varepsilon\sqrt{e}))t$, where ε represents the linear size of the initial contact zone at the onset of lipid spreading (detailed derivation in the Supporting materials and methods, section S2 Fig. S2). Fitting the experimental $A(t)$ versus time data to the expressions above yields the values of the kinetic spreading coefficient β between ~40 $\mu m^2/s$ ($\varepsilon = 0.5$ μm) and ~18 $\mu m^2/s$ ($\varepsilon = 5$ μm) (Fig. S2). These values of β shed light on the balance of forces. Recall that the OTS monolayer, which defines the hydrophobic surface, is covalently attached to the underlying glass. Thus, the spreading of lipids at the OTS surface encounters frictional resistance at the methyl-methyl interface. Approximating the friction coefficient ζ between OTS and the lipid monolayer by that between the leaflets of lipid bilayers (43), which has been variously estimated to be between 1×10^8 and 3×10^9 Ns • m^{-3} (44–46), our estimates for β translate into a rather broad range of values for the spreading power, S, between 4 and 8 mN • m^{-1} for $\zeta = 1 \times 10^8$ Ns • m^{-3} and between 120 and 240 mN • m^{-1} for $\zeta = 3 \times 10^9$ Ns • m^{-3}. These values are larger than the range of rupture

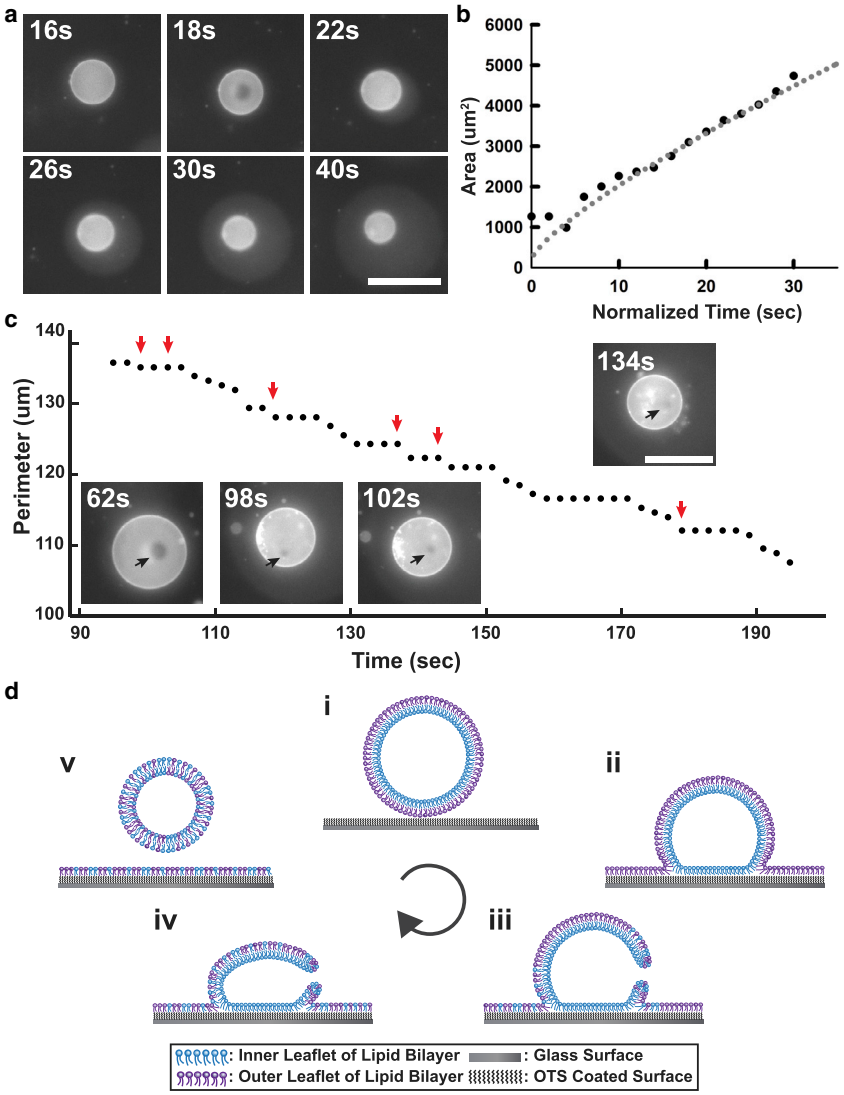

FIGURE 1 Dynamic rupture features of GUVs settling onto hydrophobic surface. (*a*) Selected frames from a video of fluorescence images of a single GUV consisting of 98% POPC and doped with 2% rhodamine-B DOPE containing 300 mM sucrose immersed in 150 mM NaCl solution incubated on hydrophobic substrate are given. Scale bars, 50 μm. (*b*) The growth of the area of the spreading patch is shown (*black dots*, experimental data). The dotted line is a numerical fit for $\beta = 18\ \mu m^2/s$ and $\varepsilon = 5\ \mu m$. (*c*) Perimeter measurements of a vesicle while ruptured onto hydrophobic surface are given. Selected images show pore of a single vesicle ruptured on the substrate. Scale bars, 50 μm. Arrows are guides to the pore presented in video. (*d*) Schematic representation of GUVs rupture on hydrophobic surface is shown. To see this figure in color, go online.

tension values (2–6 mN • m^{-1}) of equilibrated lipid bilayers, further confirming that the hydrophobic surface accelerates lipid spreading.

The considerations above suggest a mechanistic picture for the behavior of GUV at hydrophobic surfaces, such as proposed below. A hydrophobic surface in water has a large surface energy (47). The interfacial energy between the OTS surface presenting a densely packed, two-dimensional lattice of $-CH_3$ groups and water is 40–50 mN/m, which is considerably higher than expected from simple estimation of van der Waals forces (48). Because this adhesion energy is much higher than the rupture energy (5–8 mN/m) (20), thermodynamics favor the rupture of GUVs and the coverage of the hydrophobic surface with a monomolecular layer of lipids. From a dynamic consideration, the GUV rupture requires membrane poration. The structure of water in the close vicinity ($\lambda \approx 1$ nm) of the high-tension, extended hydrophobic surface is known to be highly layered (47,49), oriented with unsatisfied hydrogen bonds directed toward the surface (50), and one significantly reduced and fluctuating equilibrium density (8). Thus, it is reasonable that the GUV approaching a hydrophobic surface experiences an abrupt hydration gradient $R > \lambda$. Because hydration also affects packing of lipids (51) in the vesicular membrane, a plausible consequence of the gradient in hydration across the vesicular dimension is the lowering of the activation energy required to nucleate a defect in the water-exposed outer leaflet. This then initiates a sequence of previously identified molecular processes (31), which explain the topological transition in which GUVs abandon their closed topology furnishing lipids needed to produce the monomolecular layer covering the hydrophobic surface in water. Specifically, the surface energy of the hydrophobic surface provides the driving force, i.e., the spreading power, allowing the spreading of the lipids from the outer leaflet. This must necessarily tense the outer leaflet. The

mechanical tension in the outer monolayer, together with the mismatch in molecular densities across the two leaflets, fosters the formation of a membrane pore. The pore relaxes the membrane tension and allows for two competing processes: 1) pore-mediated lipid exchange between the two monolayers and continued spreading under the influence of the spreading power and 2) pore healing promoting pore closure. These two processes then explain the recurrent spreading we observe.

Rupture of single GUVs at extended hydrophilic surfaces

Replacing the hydrophobic surface by more commonly employed hydrophilic surface confirm previous findings and also highlight a heretofore unappreciated iterative feature of vesicle rupture. A representative time-lapse video (Video S4) and a corresponding montage of selected frames (Fig. 2 *a*; Fig. S3) of epifluorescence micrographs reveal salient features of the dynamics characterizing the morphological destabilization and topological transitions of giant vesicles at hydrophilic (i.e., glass) surface. Consistent with previous reports (24,25), we find that immediately upon contacting the surface (~10–20 s), the GUVs undergo an abrupt topological transition over subsecond timescales, abandoning their topologically closed morphology and producing characteristic heart-shaped patches adhering to the substrate surface. Surprisingly, however, we find that this vesicle-to-patch transition is not a single, catastrophic event—a feature not appreciated previously (24,25). Specifically, a single daughter GUV detaches from the surface and diffuses in the solution before re-engaging with the substrate surface merely tens of seconds later. In the majority of the cases, the daughter GUVs migrates several micrometers away from the initial patch before reinteracting with the bare substrate and producing a secondary heart-shaped patch. Interestingly, this process repeats several times before exhausting the vesicular material below the optical detection limit.

We find that this iterative nature of vesicle-to-patch transition is fully reproducible. Examining 459 independent events in 32 (n = 32) independent experiments, we discriminate three major pathways (Fig. 2, *a* and *b*). First, an overwhelming 85.6% GUVs exhibits the repetitive rupture behavior described above (Fig. 2 *c*). Second, a smaller, 13.3%, proportion of the rupture events reveal a conspicuous difference. The daughter vesicles do not migrate sufficiently far from the bilayer patches to encounter bare substrate surface (Figs. 2 *b* and S4; Videos S5 and S6). In

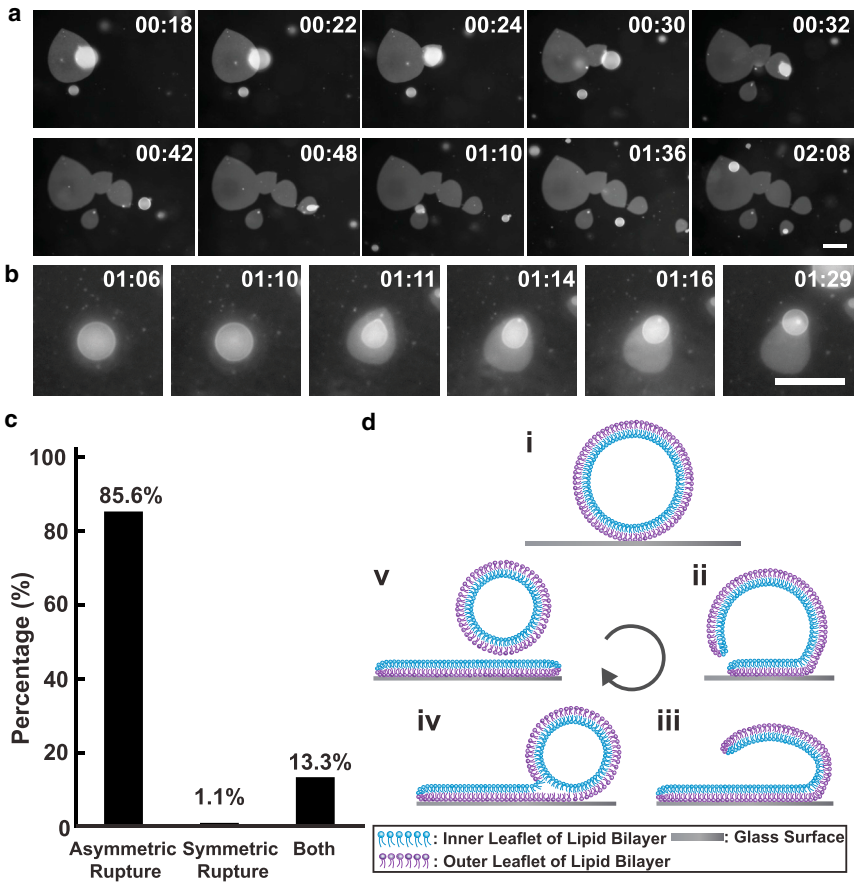

FIGURE 2 Dynamic rupture features of GUVs settling onto high-energy hydrophilic glass surface. (*a*) Selected frames from a time-lapse video of fluorescence images of a single GUV on glass substrate reveal multiple burst and reseal cycles. The GUVs were 98% POPC doped with 2% rhodamine-B DOPE. They contained 300 mM sucrose in their interior and were immersed in an aqueous solution containing 150 mM glucose and 75 mM NaCl. (*b*) Selected frames from a video of fluorescence images of a single GUV on glass substrate showing a single burst and reseal cycle are given (the GUV composition and conditions were same as in *a* except for 150 mM NaCl in the bath.) Time stamp shows minutes: seconds. Scale bars, 50 μm. (*c*) Histogram shows percentages of GUV rupturing through asymmetric pathway, symmetric pathway, or both. 459 vesicles consisting of 98% POPC doped with 2% rhodamine-B DOPE were analyzed. (*d*) A schematic representation of GUV rupture on hydrophilic glass surface is shown. To see this figure in color, go online.

these cases, the daughter vesicles fuse with the extant patch, transforming the initial heart-shaped patches into more symmetric oblong- or pear-shaped lamellar membranes. Interestingly, the rupture of GUVs here does not follow the abrupt asymmetric pathway. Rather, a gradual decrease in vesicle diameter and correspondingly a gradual expansion of the existing patch ensued, such as occurs on hydrophobic surfaces (see above). Third, in rare instances (~1%), we observe symmetric spreading on hydrophilic surfaces. But the areal spreading rate (2.6 $\mu m^2/s$) in these cases is roughly two orders of magnitude lower (Fig. S5). In all of the cases, the surface-bound membrane patches resulting from the topological transition exhibit lateral fluidity, comparable to that of fluid supported bilayers (52), as revealed by the diffusional characteristics of probe lipids (0.8 $\pm$ 0.2 $\mu m^2/s$) in microscopy-based FRAP measurements (Fig. S6; Video S7; (53)).

There are two distinct scenarios that can explain the recurrent rupture dynamics above: 1) successive ruptures of different membranes of structurally complex GUVs and 2) multiple partial ruptures of single membrane, leading to partial deposition of vesicular lipids at the substrate surface with the residual remodeling into a daughter vesicle. The former requires that the GUVs are either multilamellar, consisting of concentrically arranged lamellae in a cylindrically smectic (onion-like) organization, or oligovesicular, consisting of a hierarchy of internal "organelle" vesicles (54,55). Although the electroformation method used in this study has been shown to yield predominantly unilamellar vesicles (>80–95%), a minority of GUVs exhibiting internal tethers and oligovesicular organization are invariably produced (56–58). Thus, the possibility that the recurrent rupture dynamics we witness arises from sequential ruptures of different lamellae or from the internal organelle vesicles merits consideration. Several independent lines of evidence support the second scenario. First, we note that although wide-field fluorescence images of GUVs in Fig. 2 do not permit us to directly discriminate between unilamellar and multilamellar vesicles, the large proportion of GUVs exhibiting multiple ruptures (~86%) already suggests that GUVs with complex architectures may not be required.

Second, to further consider the possible role of structural complexity of GUVs in facilitating multiple ruptures, we used confocal fluorescence microscopy (Fig. 3; Video S8).

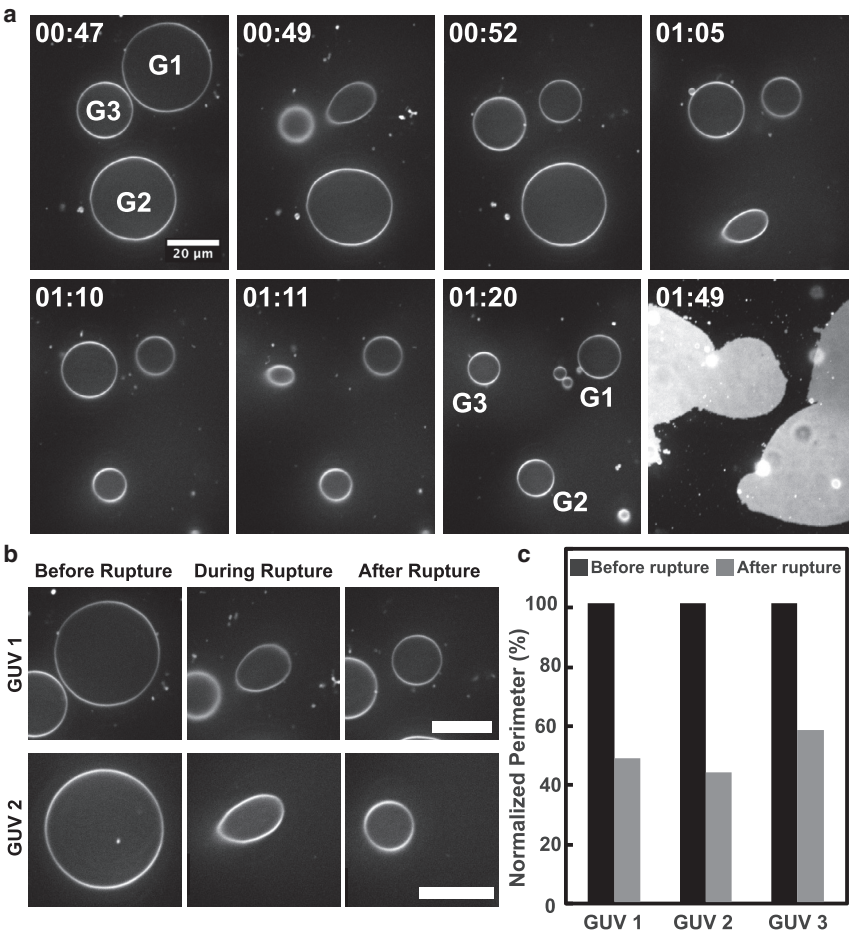

FIGURE 3 Significant size reduction of GUVs after primary rupture event. (*a*) Selected frames from a video of confocal fluorescence images of GUVs consisting of 98% POPC and doped with 2% rhodamine-B DOPE containing 300 mM sucrose immersed in 150 mM NaCl solution incubated on glass substrate are shown. Time stamp shows minutes: seconds. Scale bars, 20 μm. (*b*) Selected frames from (*a*) highlighting deformation and size reduction of GUVs before, during, and after rupture are given. (*c*) Histogram represents normalized perimeter of three individual vesicles at the equatorial plan before and after the first rupture.

We examined three different GUVs, each of which displayed no internal structure and presented a uniformly lit, sharp fluorescence boundary consistent with unilamellar architecture. The montage of images shown in Fig. 3 reveal an abrupt change in vesicle size at different times, which we interpret to correspond to the secondary vesicles produced after the first rupture event in each of the three GUVs. Notably, these secondary vesicles are considerably smaller than the original GUVs; their perimeters are estimated at roughly 40% (n = 3) of those of the initial GUVs (Fig. 3; Video S8). This transition from the initial size to the final size is also accompanied by a transient shape change characterized by the short-lived appearance of nonspherical oblong-shaped GUVs lasting several seconds. Although confocal imaging precludes simultaneous observation of the GUVs and the patch forming at the underlying glass surface, the observed change in GUV sizes (and the corresponding transient shape dynamics) are fully consistent with scenario 2, in which the rupture process induces only a partial loss of vesicular material with the remainder reassembling into secondary daughter vesicles. The alternate scenario 1, invoking complete "unbinding" of single layers from multilamellar "onion-phase" vesicles, should result in comparable sizes of patches, which was not observed. Moreover, because these GUVs did not contain internal structures, we can also rule out that the multiple ruptures originate from successive depositions of different membranes of an oligomeric vesicle (note also that oligomeric vesicles should release all internal vesicles after the first rupture producing multiple patches in the second step, which was also not observed). Third, consistent with scenario 2, we find a conservation of membrane surface area. Specifically, we find that $V_n \cong P_{n+1} + V_{n+1}$ where V_n corresponds to the surface area of the precursor GUV (nth step), V_{n+1} is the area of the secondary daughter vesicle produced in the $n + 1$ step, and P_{n+1} represents the area of the membrane patch (Fig. S7).

Taken together, the results above can be reconciled in terms of a picture of vesicular rupture as a multistep process. We propose that it arises from a competition between tendencies for membrane spreading (30,41) and pore healing triggered by adhesion-mediated membrane poration (35,59). It is orchestrated by a sequence of biophysical events including substrate mediated adhesion, poration, spreading, and resealing, together generating the rupture dynamics such as described below.

At the aqueous interface of hydrophilic surfaces, the GUVs follow a well-defined course. It begins with the approach of the GUV from the bulk solution to the glass surface. The presence of salt (>100 mM) in the aqueous solution serves to lower the electrostatic repulsion (Debye-Hückel length, $\kappa < 1$ nm) between the negatively charged glass surface at the solution pH (~5.6) and the essentially zwitterionic GUVs containing ~1 mol% negatively charged fluorescent probe (60). At the point of contact, the adhering GUV deforms to produce a flat interface or a quasihemispherical cap maximizing its contact area (A) with the surface, thereby gaining adhesion energy ($-WA$). The corresponding cost in curvature energy, determined by the bending rigidity, k, becomes manifest as a contact curvature (13), $1/R_c = (W/2\kappa)^{1/2}$, where R_c is the contact curvature along the meridian of the GUV. Taking $\kappa = 10^{-19}$ J for POPC membranes and $W = 10^{-6}$–10^{-3} J/m^2 for moderate to strong adhesion (12), the radius of the contact curvature estimates at a few tens to a few hundreds of nanometers ($14 << R_c$ (nm) ≤ 400). Because the free energy of membrane deformation is inversely proportional to the square of the radius of curvature, the contact curvature accrues significant curvature stresses locally near the rim of the interface between the GUV and the solid surface (19). Moreover, the membranes of the adhering GUVs experience an elevated membrane tension (21). These two properties, i.e., the global membrane tension and the local curvature stresses at the rim, collaborate to lower the activation energy barrier for the nucleation of a membrane pore (59). Although tension-mediated pore formation is a thermally activated, stochastic process (20,61) and the pore may, in principle, form anywhere in the membrane, the presence of local curvature stresses preferentially localize the pore formation to the vicinity of the rim (36). Furthermore, to avoid the loss of adhesion energy, it seems reasonable that the pore nucleates and spreads preferentially in the nonadhering membrane side of the rim. The free edges of the open pore then expand under the influence of the internal Laplace pressure, a process further stabilized by the adhesion with the underlying solid. This, in turn, drives spreading away from the site of pore formation, giving rise to the characteristic heart-shaped membrane patch. These considerations have been previously invoked to explain the spreading of GUVs in single rupture events (24,25).

This picture of adhesion-mediated membrane rupture, however, does not account for the repetitive rupture of single GUVs giving rise to multiple membrane patches, such as we observe (Fig. 2). This requires that the adhesive patch separate and secondary vesiculation ensue. This scenario can be reconciled by considering the competition between pore expansion and pore healing (33,35). Specifically, the pore formation creates solvent-exposed free edges. The reorientation of the edge lipids into a hemimicellar configuration (34) driven by hydrophobic forces then generates mechanical tension at the edge (γ), which for a typical lipid is on the order of tens of piconewtons (62). This edge tension can then provide a driving force for membrane healing by pore closure (32). In this case, we propose that the pore healing can occur by the joining of the edge of the unfused membrane with the membrane at the boundary separating the fused and the unfused segments of the vesicular membrane (Fig. S8). Because the fused segments of the membrane are mechanically tense with reduced thermal fluctuation, a substantial tension gradient can be expected at the junction

separating the two segments. We speculate that this tension gradient can provide the energy needed to surpass the energy barrier for the topological division required to divide a single contiguous membrane to produce a secondary, daughter vesicle (36)—mechanically akin to the process of tension-mediated membrane fission (63). The release of the daughter vesicle then allows for its diffusion into the bulk solution, and the subsequent approach to the surface. The process then repeat itself, producing multiple heart-shaped membrane patches until curvature stresses and membrane tension are insufficient to induce poration. Whether GUVs rupture in single or multiple events then depends on the balance between the two membrane-spreading and secondary vesiculation processes, both of which depend sensitively on the membrane surface adhesion energy.

It is in order here to consider whether membrane compositions that stabilize pore edges, and thus suppress the driving force for pore closure, can tip the balance between membrane spreading and secondary vesiculation, thus promoting single, catastrophic rupture. It is now well known that the presence of inverted-cone-shaped lipids (e.g., lysophospholipids), whose hydrophilic heads are larger than the hydrophobic tail(s), confer positive curvatures (the monolayer bulges toward the headgroups) to otherwise planar membranes (64,65). Their accumulation at the pore edges lowers the energetic cost of adhesion-mediated pore formation, thus, in principle, suppressing secondary vesiculation. But these wedge-shaped molecules also inhibit pore expansion (66), which is a requisite process for membrane spreading, complicating the effects of pore-stabilizing dopants in a complex, nuanced, and subtle manner. A more complete understanding of how molecular shapes of individual lipids influence the balance between pore healing and membrane spreading thus requires separate considerations, which we will separately report.

The observed iterative process of adhesion-mediated membrane rupture—reflecting a subtle balance between membrane spreading and secondary vesiculation—is phenomenologically reminiscent of the previously reported phenomenon of osmotically mediated lysis of giant vesicles (67). In the latter case, giant vesicles experiencing hypotonic stress from solute-depleted surrounding bath swell, porate, and heal in a periodic manner en route to osmotic equilibration. Specifically, the osmotic influx of water in vesicles embedded in hypotonic media accumulates membrane tension (68), which beyond a threshold tension (69) promotes vesicle lysis via pore formation and thus membrane rupture. Previous theoretical (67,70,71) and experimental (69,72–74) work demonstrates that this osmotically prompted vesicle lysis does not proceed as a singular, catastrophic event; rather, it follows a stepwise sequence of events (72,73). During each membrane rupture event, a portion of the intravesicular solute (and water) is released before the bilayer reseals, leaving the vesicle hyperosmotic, with a lower osmotic differential. This then prompts subsequent events of water influx, vesicle swelling, and rupture until sufficient intravesicular solute has been lost and the membrane is able to withstand the residual sublytic osmotic pressure without collapsing. Thus, GUVs in hypotonic media exhibit periodic oscillations in their sizes—characterized by alternating modulations of vesicular volume, tension, and solute efflux—prompted by repeated cycles of swelling and bursting (33,71,73). By analogy, this case of adhesion-mediated iterative rupture of giant vesicles at solid surfaces involves a comparable balance between membrane poration, induced by adhesion-mediated tension, and pore healing.

GUV rupture at mixed wettability patterned surfaces

The drastically different processes by which GUVs rupture, spread, and heal at hydrophilic and hydrophobic surfaces naturally raises an intriguing question: how do GUVs rupture at amphiphilic surfaces consisting both of hydrophilic and hydrophobic regions? To address this question, we prepared surfaces presenting binary, microscopic spatial patterns of surface wettability consisting of alternating 100 μm (roughly 5$\times$ the size of a representative GUV) wide stripes of hydrophilic silica and hydrophobic surfaces. Monitoring the behavior of single GUVs at these surfaces in real time (Fig. 4; Video S9) revealed an unexpected behavior characterized by three salient features. First, the GUV rupture became localized almost exclusively to the pattern boundaries separating hydrophilic and hydrophobic regions of the solid surface. The origins of this enhanced attractiveness for GUV adhesion at the wetting boundary are at present not clear to us. We speculate the role of the wettability gradient. A hydrophilic surface immersed in water is uniformly covered by water, whereas the aqueous interface of a macroscopic hydrophobic surface is essentially "dry." In other words, at the spatial boundaries of chemically patterned surfaces, water structure must undergo a rather drastic structural change. This, in turn, produces an epistructural tension (75)—the reversible work required to span the aqueous interface of the patterned surface—which provides a driving force for an enhancement in GUV adhesion. Second, the vesicles bound to the pattern boundaries at the substrate surface, quite remarkably, spread in a strikingly asymmetric fashion preferentially covering the hydrophilic regions of the patterned surface. A consequence of this spatially patterned mode of vesicle-surface interaction is the formation of elliptically deformed bilayer patches on the hydrophilic channels, lithographically defined by the geometric properties of the underlying amphiphilic surface. We reason that this selection is kinetic, arising from faster spreading kinetics at hydrophilic surfaces (30,42). Third, in this mode of GUV rupture and spreading, we find little or no evidence for the repetitive spreading, indicating that the spreading overwhelms the competition

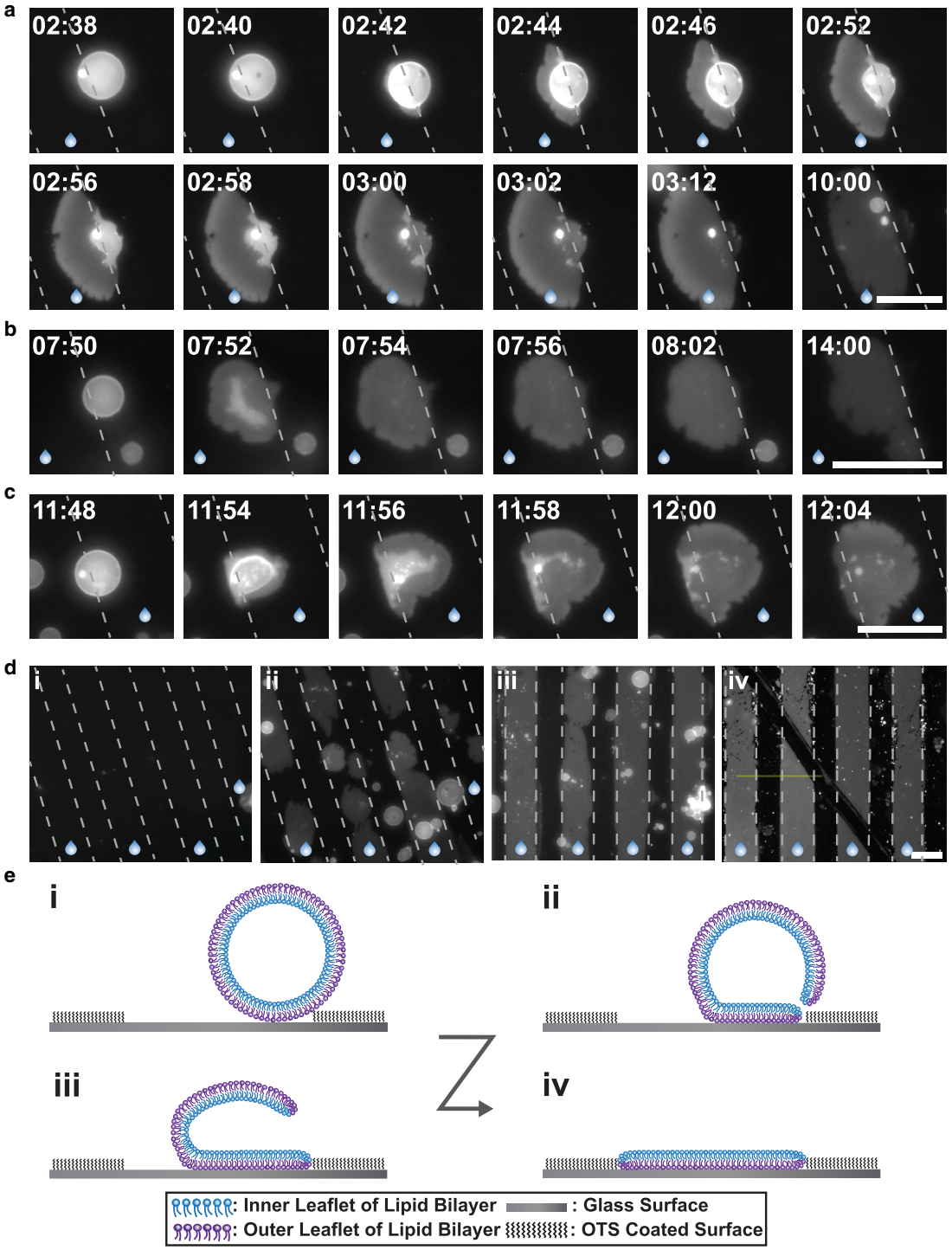

FIGURE 4 GUV destabilization on a pattern of hydrophilic and OTS-coated hydrophobic substrate. (*a–c*) show a time-lapse sequence of fluorescence images of different GUVs consisting of 98% POPC and doped with 2% rhodamine-B DOPE containing 300 mM sucrose upon immersion in the external dispersion medium containing 150 mM NaCl solution and incubated on a pattern of hydrophilic and OTS-coated hydrophobic substrate. Time stamp shows minutes: seconds. Scale bars, 50 μm. (*d*) Images of the patterned surface (i) before, (ii) after 5 min, (iii) after 35 min of incubation of the GUVs on pattern substrate, and (iv) after rinsing with water on the patterned surface are shown. Dash lines are guide to interface between hydrophilic and hydrophobic area. Water droplets are guide to hydrophilic area. Scale bars, 50 μm. (*e*) Schematic representation of GUVs rupture on the patterned hydrophilic and hydrophobic substrate is given. To see this figure in color, go online.

from the pore healing (see above). Based on these characteristics, we propose that chemically structured surfaces or hydrophilic surfaces impregnated with hydrophobic "impurities" may foster GUV adhesion, localize GUV binding at predetermined spatial locations, and suppress the recurrent rupture dynamics, thereby promoting complete membrane spreading in single bursts.

SUPPORTING MATERIAL

Supporting Material can be found online at https://doi.org/10.1016/j.bpj.2021.01.006.

AUTHOR CONTRIBUTIONS

All co-authors contributed to the design of the study. A.N.P. led the effort. V.N.N. trained the undergraduate researchers (Y.D., Z.Y., N.W.-T., and V.P.S.) and performed initial experiments. S.P. quantified the spreading rates. W.-C.S. reproduced initial results, carried out supporting experiments, and analyzed data. A.N.P. and W.-C.S. wrote the manuscript.

ACKNOWLEDGMENTS

We thank the MCB Light Microscopy Imaging Facility, which is a UC-Davis Campus Core Research Facility, for the use of this microscope. We are grateful to P. Rangamani for an insightful critique of the manuscript.

This work is supported by a grant from the National Science Foundation (DMR-1810540). The 3i Marianas spinning disk confocal used in this study was purchased using National Institutes of Health Shared Instrumentation Grant 1S10RR024543-01.

REFERENCES

1. Walde, P., K. Cosentino, …, P. Stano. 2010. Giant vesicles: preparations and applications. *ChemBioChem.* 11:848–865.
2. Menger, F. M., and M. I. Angelova. 1998. Giant vesicles: imitating the cytological processes of cell membranes. *Acc. Chem. Res.* 31:789–797.
3. Dimova, R., S. Aranda, …, R. Lipowsky. 2006. A practical guide to giant vesicles. Probing the membrane nanoregime via optical microscopy. *J. Phys. Condens. Matter.* 18:S1151–S1176.
4. Morales-Penningston, N. F., J. Wu, …, G. W. Feigenson. 2010. GUV preparation and imaging: minimizing artifacts. *Biochim. Biophys. Acta.* 1798:1324–1332.
5. Dimova, R., and C. M. Marques. 2020. The Giant Vesicle Book. CRC Press, Boca Raton, FL.
6. Lipowsky, R. 1991. The conformation of membranes. *Nature.* 349:475–481.
7. Singer, S. J., and G. L. Nicolson. 1972. The fluid mosaic model of the structure of cell membranes. *Science.* 175:720–731.
8. Chandler, D. 2005. Interfaces and the driving force of hydrophobic assembly. *Nature.* 437:640–647.
9. Hénon, S., G. Lenormand, …, F. Gallet. 1999. A new determination of the shear modulus of the human erythrocyte membrane using optical tweezers. *Biophys. J.* 76:1145–1151.
10. Hochmuth, R. M., and R. E. Waugh. 1987. Erythrocyte membrane elasticity and viscosity. *Annu. Rev. Physiol.* 49:209–219.
11. Svetina, S., and B. Zeks. 1989. Membrane bending energy and shape determination of phospholipid vesicles and red blood cells. *Eur. Biophys. J.* 17:101–111.
12. Lipowsky, R., and U. Seifert. 1991. Adhesion of vesicles and membranes. *Mol. Cryst. Liq. Cryst. (Phila. Pa.).* 202:17–25.
13. Seifert, U., and R. Lipowsky. 1990. Adhesion of vesicles. *Phys. Rev. A.* 42:4768–4771.
14. Rädler, J. O., T. J. Feder, …, E. Sackmann. 1995. Fluctuation analysis of tension-controlled undulation forces between giant vesicles and solid substrates. *Phys. Rev. E Stat. Phys. Plasmas Fluids Relat. Interdiscip. Topics.* 51:4526–4536.
15. Murrell, M. P., R. Voituriez, …, M. L. Gardel. 2014. Liposome adhesion generates traction stress. *Nat. Phys.* 10:163–169.
16. Bernard, A. L., M. A. Guedeau-Boudeville, …, J. M. di Meglio. 2000. Strong adhesion of giant vesicles on surfaces: dynamics and permeability. *Langmuir.* 16:6809–6820.
17. Zhao, J., J. Wu, and S. L. Veatch. 2013. Adhesion stabilizes robust lipid heterogeneity in supercritical membranes at physiological temperature. *Biophys. J.* 104:825–834.
18. Gordon, V. D., M. Deserno, …, W. C. K. Poon. 2008. Adhesion promotes phase separation in mixed-lipid membranes. *Europhys. Lett.* 84:48003.
19. Zhdanov, V. P. 2015. Mechanism of rupture of single adsorbed vesicles. *Chem. Phys. Lett.* 641:20–22.
20. Evans, E., V. Heinrich, …, W. Rawicz. 2003. Dynamic tension spectroscopy and strength of biomembranes. *Biophys. J.* 85:2342–2350.
21. Takáts-Nyeste, A., and I. Derényi. 2014. Rupture of lipid vesicles near solid surfaces. *Phys. Rev. E Stat. Nonlin. Soft Matter Phys.* 90:052710.
22. Lenz, P., J. M. Johnson, …, S. G. Boxer. 2006. Tension-induced pore formation and leakage in adhering vesicles. *Europhys. Lett.* 75:659–665.
23. Johnson, J. M., T. Ha, …, S. G. Boxer. 2002. Early steps of supported bilayer formation probed by single vesicle fluorescence assays. *Biophys. J.* 83:3371–3379.
24. Hamai, C., P. S. Cremer, and S. M. Musser. 2007. Single giant vesicle rupture events reveal multiple mechanisms of glass-supported bilayer formation. *Biophys. J.* 92:1988–1999.
25. Kataoka-Hamai, C., and T. Yamazaki. 2015. Induced rupture of vesicles adsorbed on glass by pore formation at the surface-bilayer interface. *Langmuir.* 31:1312–1319.
26. Kataoka-Hamai, C., and K. Kawakami. 2019. Interaction mechanisms of giant unilamellar vesicles with hydrophobic glass surfaces and silicone oil-water interfaces: adsorption, deformation, rupture, dynamic shape changes, internal vesicle formation, and desorption. *Langmuir.* 35:16136–16145.
27. Aoki, P. H. B., A. P. Schroder, …, C. M. Marques. 2015. Bioadhesive giant vesicles for monitoring hydroperoxidation in lipid membranes. *Soft Matter.* 11:5995–5998.
28. Thalmann, F., V. Billot, and C. M. Marques. 2011. Lipid bilayer adhesion on sparse DNA carpets: theoretical analysis of membrane deformations induced by single-end-grafted polymers. *Phys. Rev. E Stat. Nonlin. Soft Matter Phys.* 83:061922.
29. Howland, M. C., A. R. Sapuri-Butti, …, A. N. Parikh. 2005. Phospholipid morphologies on photochemically patterned silane monolayers. *J. Am. Chem. Soc.* 127:6752–6765.
30. Sanii, B., and A. N. Parikh. 2007. Surface-energy dependent spreading of lipid monolayers and bilayers. *Soft Matter.* 3:974–977.
31. Zan, G. H., C. Tan, …, M. Lösche. 2012. Hemifusion of giant unilamellar vesicles with planar hydrophobic surfaces: a fluorescence microscopy study. *Soft Matter.* 8:10877–10886.
32. Brochard-Wyart, F., P. G. de Gennes, and O. Sandre. 2000. Transient pores in stretched vesicles: role of leak-out. *Physica A.* 278:32–51.
33. Sandre, O., L. Moreaux, and F. Brochard-Wyart. 1999. Dynamics of transient pores in stretched vesicles. *Proc. Natl. Acad. Sci. USA.* 96:10591–10596.
34. Litster, J. D. 1975. Stability of lipid bilayers and red blood-cell membranes. *Phys. Lett. A.* 53:193–194.

35. Karatekin, E., O. Sandre, and F. Brochard-Wyart. 2003. Transient pores in vesicles. *Polym. Int.* 52:486–493.
36. Wu, H. L., P. Y. Chen, …, Y. J. Sheng. 2013. Vesicle deposition on hydrophilic solid surfaces. *Soft Matter.* 9:1908–1919.
37. Angelova, M. I., and D. S. Dimitrov. 1986. Liposome electroformation. *Faraday Discuss. Chem. Soc.* 81:303–311.
38. Kang, M., C. A. Day, …, E. DiBenedetto. 2012. Simplified equation to extract diffusion coefficients from confocal FRAP data. *Traffic.* 13:1589–1600.
39. Baumgart, T., G. Hunt, …, G. W. Feigenson. 2007. Fluorescence probe partitioning between Lo/Ld phases in lipid membranes. *Biochim. Biophys. Acta.* 1768:2182–2194.
40. Czolkos, I., Y. Erkan, …, O. Orwar. 2007. Controlled formation and mixing of two-dimensional fluids. *Nano Lett.* 7:1980–1984.
41. Radler, J., H. Strey, and E. Sackmann. 1995. Phenomenology and kinetics of lipid bilayer spreading on hydrophilic surfaces. *Langmuir.* 11:4539–4548.
42. Nissen, J., S. Gritsch, …, J. O. Radler. 1999. Wetting of phospholipid membranes on hydrophilic surfaces - concepts towards self-healing membranes. *Eur. Phys. J. B.* 10:335–344.
43. Merkel, R., E. Sackmann, and E. Evans. 1989. Molecular friction and epitactic coupling between monolayers in supported bilayers. *J. Phys. (Paris).* 50:1535–1555.
44. Evans, E., and A. Yeung. 1994. Hidden dynamics in rapid changes of bilayer shape. *Chem. Phys. Lipids.* 73:39–56.
45. Fournier, J. B., N. Khalifat, …, M. I. Angelova. 2009. Chemically triggered ejection of membrane tubules controlled by intermonolayer friction. *Phys. Rev. Lett.* 102:018102.
46. Horner, A., S. A. Akimov, and P. Pohl. 2013. Long and short lipid molecules experience the same interleaflet drag in lipid bilayers. *Phys. Rev. Lett.* 110:268101.
47. Lee, C. Y., J. A. McCammon, and P. J. Rossky. 1984. The structure of liquid water at an extended hydrophobic surface. *J. Chem. Phys.* 80:4448–4455.
48. Christenson, H. K., and P. M. Claesson. 2001. Direct measurements of the force between hydrophobic surfaces in water. *Adv. Colloid Interface Sci.* 91:391–436.
49. Israelachvili, J. N., and R. M. Pashley. 1983. Molecular layering of water at surfaces and origin of repulsive hydration forces. *Nature.* 306:249–250.
50. Fumagalli, L., A. Esfandiar, …, A. K. Geim. 2018. Anomalously low dielectric constant of confined water. *Science.* 360:1339–1342.
51. Hristova, K., and S. H. White. 1998. Determination of the hydrocarbon core structure of fluid dioleoylphosphocholine (DOPC) bilayers by x-ray diffraction using specific bromination of the double-bonds: effect of hydration. *Biophys. J.* 74:2419–2433.
52. Castellana, E. T., and P. S. Cremer. 2006. Solid supported lipid bilayers: from biophysical studies to sensor design. *Surf. Sci. Rep.* 61:429–444.
53. Axelrod, D., D. E. Koppel, …, W. W. Webb. 1976. Mobility measurement by analysis of fluorescence photobleaching recovery kinetics. *Biophys. J.* 16:1055–1069.
54. Okumura, Y., T. Nakaya, …, K. Urita. 2011. Giant vesicles with membranous microcompartments. *Langmuir.* 27:3279–3282.
55. Menger, F. M., S. J. Lee, and J. S. Keiper. 1996. Differentiating unilamellar, multilamellar, and oligovesicular vesicles using a fluorescent dye. *Langmuir.* 12:4479–4480.
56. Rodriguez, N., F. Pincet, and S. Cribier. 2005. Giant vesicles formed by gentle hydration and electroformation: a comparison by fluorescence microscopy. *Colloids Surf. B Biointerfaces.* 42:125–130.
57. Akashi, K., H. Miyata, …, K. Kinosita, Jr. 1996. Preparation of giant liposomes in physiological conditions and their characterization under an optical microscope. *Biophys. J.* 71:3242–3250.
58. Mathivet, L., S. Cribier, and P. F. Devaux. 1996. Shape change and physical properties of giant phospholipid vesicles prepared in the presence of an AC electric field. *Biophys. J.* 70:1112–1121.
59. Evans, E., and B. A. Smith. 2011. Kinetics of hole nucleation in biomembrane rupture. *New J. Phys.* 13:29.
60. Anderson, T. H., Y. Min, …, J. N. Israelachvili. 2009. Formation of supported bilayers on silica substrates. *Langmuir.* 25:6997–7005.
61. Ting, C. L., D. Appelö, and Z. G. Wang. 2011. Minimum energy path to membrane pore formation and rupture. *Phys. Rev. Lett.* 106:168101.
62. Portet, T., and R. Dimova. 2010. A new method for measuring edge tensions and stability of lipid bilayers: effect of membrane composition. *Biophys. J.* 99:3264–3273.
63. Zhang, G., and M. Müller. 2017. Rupturing the hemi-fission intermediate in membrane fission under tension: reaction coordinates, kinetic pathways, and free-energy barriers. *J. Chem. Phys.* 147:064906.
64. McMahon, H. T., and J. L. Gallop. 2005. Membrane curvature and mechanisms of dynamic cell membrane remodelling. *Nature.* 438:590–596.
65. Zimmerberg, J., and M. M. Kozlov. 2006. How proteins produce cellular membrane curvature. *Nat. Rev. Mol. Cell Biol.* 7:9–19.
66. Ciechonska, M., and R. Duncan. 2014. Lysophosphatidylcholine reversibly arrests pore expansion during syncytium formation mediated by diverse viral fusogens. *J. Virol.* 88:6528–6531.
67. Koslov, M. M., and V. S. Markin. 1984. A theory of osmotic lysis of lipid vesicles. *J. Theor. Biol.* 109:17–39.
68. Needham, D., and R. S. Nunn. 1990. Elastic deformation and failure of lipid bilayer membranes containing cholesterol. *Biophys. J.* 58:997–1009.
69. Hallett, F. R., J. Marsh, …, J. M. Wood. 1993. Mechanical properties of vesicles. II. A model for osmotic swelling and lysis. *Biophys. J.* 64:435–442.
70. Chabanon, M., J. C. S. Ho, …, P. Rangamani. 2017. Pulsatile lipid vesicles under osmotic stress. *Biophys. J.* 112:1682–1691.
71. Popescu, D., and A. G. Popescu. 2008. The working of a pulsatory liposome. *J. Theor. Biol.* 254:515–519.
72. Ertel, A., A. G. Marangoni, …, J. M. Wood. 1993. Mechanical properties of vesicles. I. Coordinated analysis of osmotic swelling and lysis. *Biophys. J.* 64:426–434.
73. Peterlin, P., V. Arrigler, …, H. Diamant. 2012. Law of corresponding states for osmotic swelling of vesicles. *Soft Matter.* 8:2185–2193.
74. Oglęcka, K., P. Rangamani, …, A. N. Parikh. 2014. Oscillatory phase separation in giant lipid vesicles induced by transmembrane osmotic differentials. *eLife.* 3:e03695.
75. Fernández, A. 2012. Epistructural tension promotes protein associations. *Phys. Rev. Lett.* 108:188102.